THE ASTROPHYSICAL JOURNAL, 508:539–550, 1998 December 1

INFRARED OBSERVATIONS OF NEBULAR EMISSION LINES FROM GALAXIES AT $z \simeq 3$

MAX PETTINI
Royal Greenwich Observatory, Madingley Road, Cambridge, CB3 0EZ, England, UK
MELINDA KELLOGG AND CHARLES C. STEIDEL[1,2]
Palomar Observatory, Caltech 105-24, Pasadena, CA 91125
MARK DICKINSON[3,4]
Department of Physics and Astronomy, The Johns Hopkins University, Baltimore, MD 21218
KURT L. ADELBERGER
Palomar Observatory, Caltech 105-24, Pasadena, CA 91125
AND
MAURO GIAVALISCO[5]
The Carnegie Observatories, 813 Santa Barbara Street, Pasadena, CA 91101
Received 1998 March 12; accepted 1998 July 9

ABSTRACT

We present the first results from a program of near-infrared spectroscopy aimed at studying the familiar rest-frame optical emission lines from the H II regions of Lyman break galaxies at $z \simeq 3$. By targeting redshifts that bring the lines of interest into gaps between the strong OH sky emission, we have been successful in detecting Balmer and [O III] emission lines in all five galaxies observed so far with CGS4 on UKIRT. The typical line fluxes are a few times 10^{-17} ergs s^{-1} cm^{-2}, approximately 1 order of magnitude lower than the limits reached with wide-field narrowband imaging surveys. For a Salpeter initial mass function and a $H_0 = 70$ km s^{-1} Mpc^{-1}, $q_0 = 0.1$ cosmology, the Hβ luminosities uncorrected for dust extinction imply star formation rates of 20–270 $M_\odot$ yr^{-1}; these values are greater than those that may have been deduced from the ultraviolet continuum luminosities at 1500 Å by factors of between $\sim$0.7 and $\sim$7. Uncertainties in the shape of the reddening curve and in the intrinsic UV continuum slope do not yet allow us to assess accurately the level of dust extinction; however, on the basis of the present limited sample, it appears that an extinction of 1–2 mag at 1500 Å may be typical of Lyman break galaxies. This value is consistent with recent estimates of dust obscuration in star-forming galaxies at $z \leq 1$ and does not require a substantial revision of the broad picture of star formation over the Hubble time proposed by Madau and coworkers in 1996. In four out of five cases the velocity dispersion of the emission line gas is $\sigma \simeq 70$ km s^{-1}, while in the fifth the line widths are nearly three times larger. Virial masses $M_{\rm vir} \approx (1\text{–}5) \times 10^{10}\ M_\odot$ are suggested, but both velocities and masses could be higher, because our observations are only sensitive to the brightest cores of these systems where the line widths may not sample the full gravitational potential. The relative redshifts of interstellar absorption, nebular emission, and Lyα emission lines differ by several hundred km s^{-1} and suggest that large-scale outflows may be a common characteristic of Lyman break galaxies. The forthcoming availability of high-resolution infrared spectrographs on large telescopes will soon allow all of these questions to be addressed in much greater detail.

Subject headings: cosmology: observations — galaxies: evolution — galaxies: starburst — infrared: galaxies

1. INTRODUCTION

Star-forming galaxies at redshift $z \simeq 3$ are now being discovered in large numbers from deep imaging surveys designed to reveal the break in their spectral energy distribution caused by the limit of the Lyman series of neutral hydrogen at 912 Å (Steidel, Pettini, & Hamilton 1995; Steidel et al. 1996; Lowenthal et al. 1997). At $z = 3$, optical wavelengths sample the rest-frame ultraviolet continuum, which, being produced primarily by O and early B type stars, is a measure of the instantaneous star formation rate (SFR). Thus, by constructing the ultraviolet luminosity function of galaxies in different redshift intervals, it has become possible to sketch the global history of star formation (and associated metal production) in the universe over $\sim$90% of the Hubble time (Madau, Pozzetti, & Dickinson 1998).

In principle, the ultraviolet continuum is a more direct avenue to the SFR than other commonly used indicators such as the Balmer lines, which measure the reprocessed ionizing flux from the most massive stars, and the far-infrared luminosity due to grain emission. Concerns remain, however, regarding the extent to which the observed ultraviolet luminosities are attenuated by the dust that is likely to be associated with the star-forming regions, given that even relatively small column densities of dust can modify substantially the emergent spectral energy distribution in the far-UV.

The magnitude of the dust correction appropriate to Lyman break galaxies is currently the subject of considerable debate. On the one hand, there are claims that the

[1] Alfred P. Sloan Foundation Fellow.
[2] NSF Young Investigator.
[3] Allan C. Davis Fellow.
[4] Also Space Telescope Science Institute, 3700 San Martin Drive, Baltimore, MD 21218.
[5] Hubble Fellow.

ultraviolet continuum slope and UV-optical spectral energy distribution (SED) imply that the typical $z \simeq 3$ galaxy suffers a factor of $\gtrsim 10$ extinction at 1500 Å (Meurer et al. 1997; Sawicki & Yee 1998), although other analyses (e.g., Trager et al. 1997) arrive at more modest estimates (factors of 2–6) from similar data. The first results from searches at submillimeter wavelengths have been interpreted as evidence for a significant population of dust-obscured star-forming galaxies at $z > 2$ (Blain et al. 1998), but the present uncertainties in the surface density of submillimeter sources and in their redshifts make such conclusions still tentative. Higher metal production rates than those implied by the (uncorrected) ultraviolet luminosity density at high redshift have also been advocated to explain the lack of evolution in the Fe abundance of rich galaxy clusters up to $z \sim 0.3$ (Mushotzky & Loewenstein 1997; Renzini 1997).

On the other hand, dust obscuration does not appear to be a major problem for galaxies at $z \lesssim 1$. Observations of the infrared continuum with the *Infrared Space Observatory* (Flores et al. 1998) and of the Hα emission line (Tresse & Maddox 1998; Glazebrook et al. 1999) indicate that the typical correction to the near-UV continuum luminosity at 2800 Å is at most a factor of 2 (see also Treyer et al. 1998). Similarly, the initial results from a survey of Hα emission associated with damped Lyα galaxies at $z \simeq 2.5$ by Bechtold et al. (1998) do not point to a significantly higher SFR density than that predicted by Madau et al. (1998).

This confusing situation is unlikely to be settled simply by improved measurements of the ultraviolet spectra of high-redshift galaxies. As discussed below, uncertainties in the shapes of both the unattenuated SED and the reddening curve limit the accuracy of even the most careful estimates of ultraviolet extinction. A more profitable approach may be to search for Balmer emission lines, particularly Hα and Hβ, associated with known galaxies at $z \simeq 3$. Since the effects of dust are less severe at rest-frame optical wavelengths, a comparison between the SFR implied by the Balmer lines and by the ultraviolet continuum should lead to estimates of dust obscuration that are less model-dependent. An added incentive is the possibility of obtaining from the widths of the nebular lines direct estimates of the masses of the galaxies that, as argued by Steidel et al. (1996), cannot be reliably deduced from consideration of the ultraviolet interstellar absorption lines alone. Knowledge of the masses associated with Lyman break galaxies would make it possible to use their clustering properties to discriminate between different cosmologies (Adelberger et al. 1998; Steidel et al. 1998b).

With these goals in mind, we have begun a pilot program aimed at detecting nebular emission lines from galaxies at $z \simeq 3$; in this paper we report on the initial results of this work. The brighter objects in our spectroscopically confirmed sample of Lyman break galaxies are within reach of high-resolution near-infrared spectrographs on 4 m telescopes, and indeed we have detected Balmer and/or [O III] emission lines in every one of the five galaxies observed so far. With the forthcoming availability of similar spectrographs on 8–10 m telescopes, such detections will become routine and may eventually resolve the vexed question of dust obscuration at high redshift.

2. OBSERVATIONS AND DATA REDUCTION

The near-IR sky is dominated by strong and highly variable airglow emission from the hydroxyl radical (e.g., Ramsay, Mountain, & Geballe 1992), which normally precludes spectroscopic observations of faint sources. At a resolving power $R \gtrsim 2500$, however, the OH lines are resolved, and a significant portion of the spectrum, particularly in the *K*-band, becomes accessible for work. With the large samples of Lyman break galaxies now available, it is possible to choose objects at favorable redshifts in such a way that the nebular lines of interest fall in gaps between the skylines. The CGS4 spectrograph on the United Kingdom Infrared Telescope (UKIRT) on Mauna Kea, Hawaii, with a 256×256 InSb array provides both the spectral resolution and the wavelength coverage necessary for a search for Hβ and [O III] $\lambda\lambda$4959, 5007 at $z \simeq 3$.

Table 1 gives details of the galaxies observed. From our Keck Low-Resolution and Imaging Spectrograph (LRIS) spectra, which are reproduced in Figure 1, we measure *two* values of redshift for each galaxy, from Lyα emission (when present) and from the interstellar absorption lines; they are listed in columns (4) and (5), respectively (all redshifts are vacuum heliocentric). As discussed below (§ 5), Lyα emission is generally redshifted relative to the absorption lines by up to several hundred km s^{-1}, presumably reflecting large-scale outflows in the interstellar media of these galaxies (Kunth et al. 1998). Details of the Keck observations and of the optical and infrared imaging from which the $\mathscr{R}$ mag and colors in Table 1 were derived will be presented elsewhere. Here we concentrate on UKIRT observations in the *K*-band aimed at detecting Hβ and [O III] emission lines at $z \simeq 3$ and in one case, Q0201+113 B13, Hα at $z \simeq 2.2$.[6]

The data were obtained over three observing runs in 1996 September, and 1997 October and November. In 1996 we used the 150 mm focal length camera and 150 grooves mm^{-1} grating (in second order) to give a dispersion of 200 Å mm^{-1} (6 Å pixel^{-1}); with a 1.″2 wide entrance slit and half-pixel stepping of the spectrum on the detector to improve the sampling, we achieved a resolving power $R \simeq 2600$ corresponding to FWHM $\simeq 8$ Å in the *K*-band. In the 1997 observing runs, the improved image quality delivered by the new UKIRT tip-tilt system allowed us to use the longer focal length (300 mm) camera; the corresponding resolution—with the same grating and slit width as in 1996—was FWHM $\simeq 6$ Å.

At the telescope we followed standard observing techniques; a good description of the finer points to be taken into account when observing faint objects with UKIRT and CGS4 is given by Eales & Rawlings (1993). The galaxies were acquired by blind offsets from nearby stars whose relative positions we had previously measured from our own CCD images with a typical accuracy of $\pm 0.''2$. We only used offsets stars within $\approx 2'$ of the galaxies to make sure that both galaxy and star would fall on the dichroic filter used to direct the optical light to the guiding system. The spectra were recorded on two sets of rows on the detector separated by $\sim 20''$; the object was beam switched between these two positions on the slit in a A-B-B-A sequence with 600 s integration at each position.

The choice of 600 s as the length of an individual exposure (significantly longer than is normally the case when

[6] Q0201+113 B13 does not qualify as a Lyman break galaxy according to our usual photometric selection criteria. It is one of several galaxies in the tail of the redshift distribution of our sample, discovered in the process of exploring the boundaries for Lyman break galaxies in the $(U_n - G)$ vs. $(G - \mathscr{R})$ color plane (Steidel et al. 1995).

TABLE 1

GALAXIES OBSERVED

Name (1)	R.A.[a] (2)	Decl.[a] (3)	$z_{Ly\alpha}$[b] (4)	z_{abs}[c] (5)	$\mathscr{R}$ (6)	$(G-\mathscr{R})$ (7)	$(\mathscr{R}-K_{AB})$[d] (8)	Exposure Time (s) (9)	UKIRT Observating Run (10)
Q0000−263 D6	00 03 23.8	−26 02 49	2.971	2.961	22.88	0.45	0.42	21600	1996 Sep
Q0201+113 C6.....	02 03 41.8	+11 34 42	...	3.053	23.90	0.58	0.50	18000	1996 Sep
Q0201+113 B13.....	02 03 49.3	+11 36 11	...	2.168	23.43	−0.06	0.93	39500	1997 Oct–Nov
B2 0902+343 C6	09 05 20.5	+34 09 08	3.099	3.080	24.13	0.45	1.21	21600	1997 Nov
DSF 2237+116 C2.....	22 40 08.3	+11 49 05	3.333	3.319	23.55	1.13	1.25	33600	1997 Nov

NOTE.—Units of right ascension are hours, minutes, and seconds, and units of declination are degrees, arcminutes, and arcseconds.

[a] J2000 coordinates.

[b] Redshift of Lyα emission when present.

[c] Redshift of interstellar absorption lines.

[d] All magnitudes are in the AB system; $K_{AB} = K_s + 1.86$, where K_s is the magnitude on the Vega scale.

working in the infrared) was driven by the need to minimize the read-out noise of the detector relative to the sky noise in the dark regions of sky between the OH lines where the Balmer and [O III] emission lines are expected to fall. The penalty that one pays for such long exposures is that some of the OH lines saturate or, in any case, vary sufficiently between successive exposures to make it impossible to subtract them out properly. In the circumstances, we preferred this course of action (relative to shorter exposures), because our observing strategy was specifically aimed at *avoiding* the sky emission lines.

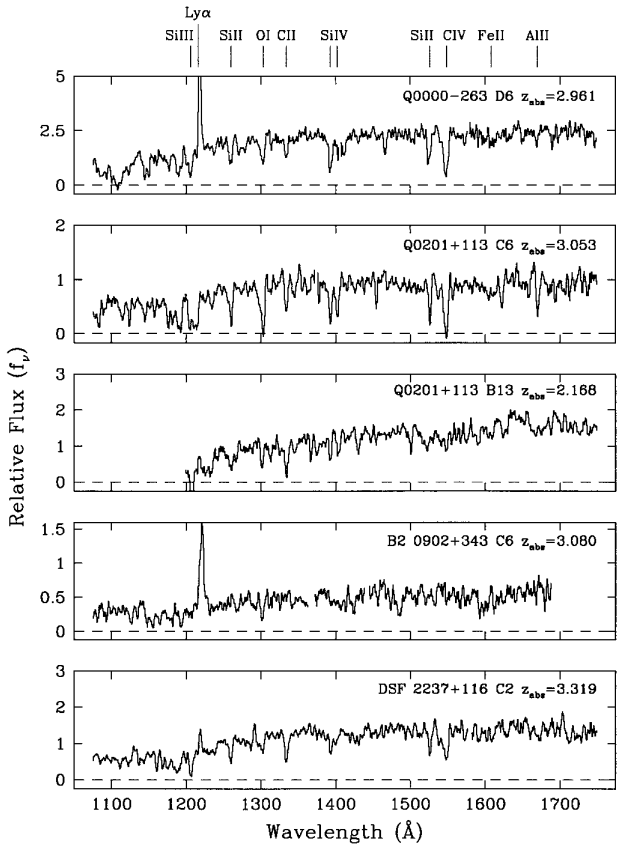

FIG. 1.—LRIS optical spectra of the five galaxies studied in this work. Each spectrum is shown in the rest frame at the redshift of the interstellar absorption lines; the flux scale is arbitrary. The positions of the most prominent interstellar lines are indicated at the top. The spectra have been smoothed with a kernel of width 12 Å (the spectral resolution) for display.

After two sequences of four 600 s exposures (i.e., approximately every 4800 s), we returned to the offset star and realigned the optical and infrared beams (to take into account the effects of differential atmospheric refraction) before repeating the blind offset procedure. With total exposure times of between 18,000 and 40,000 s (see Table 1), the final spectra are the sum of many such groups of four exposures. Between successive nights we stepped the grating so as to shift the spectra by a few pixels along the rows of the detector; this reduces the residual fixed pattern noise after flat-fielding. In general, we summed only data obtained on photometric nights with $\lesssim 1''$ seeing. One exception are the 1997 October observations of Q0201+113 B13, which were obtained in patchy cloud and $1''$–$1''.5$ seeing but which were nevertheless found to improve the final signal-to-noise ratio (S/N) of the spectrum.

Wavelength calibration was by reference to the emission line spectra of Ar and Kr hollow-cathode lamps internal to the spectrograph; we further used the sky OH emission lines to monitor any wavelength shifts during the long series of exposures. Observations of standard stars, normally of spectral type A0, provided an absolute flux scale for the galaxy spectra. The major steps of the data reduction procedure are also well described by Eales & Rawlings (1993). Briefly, the UKIRT CGS4 data reduction system provides flat-fielded two-dimensional images of each group of four exposures where the sky background has been subtracted by subtracting the sum of the two frames with the object at position B from the sum of the two frames with the object at A. We used IRAF to wavelength-calibrate and rebin these two-dimensional images to a linear scale; we then removed the sky residuals (due mainly to temporal variations in the OH lines) in each wavelength bin by fitting the background along the slit with a first-order cubic spline. The last steps involved extracting the galaxy spectra at positions A and B, multiplying B by −1 (since the initial UKIRT processing described above produces a *negative* signal at position B), and adding the resultant two spectra. We then coadded the extractions from each group of four exposures to produce the final spectra. In general we found that using weighted extraction and coadding algorithms made little difference to the final S/N.

2.1. *Results*

Figures 2 and 3 show portions of the UKIRT spectra obtained in 1996 and 1997, respectively; in Figure 4 we have reproduced the inner three cross sections of the reduced

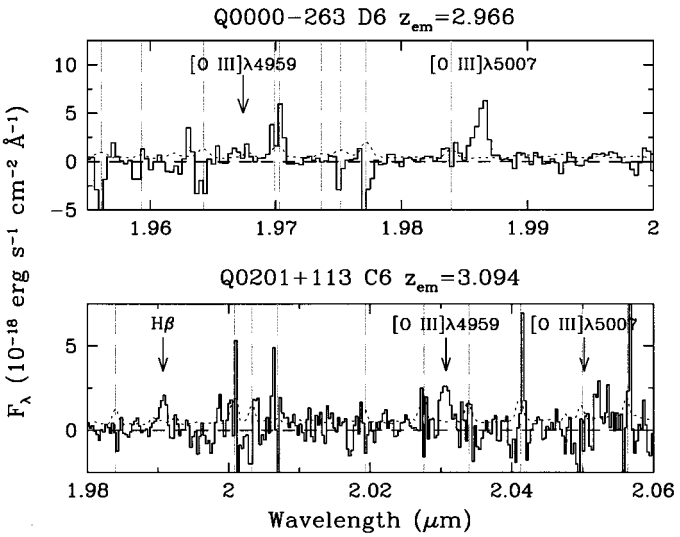

FIG. 2.—Portions of the UKIRT spectra of $z \simeq 3$ Lyman break galaxies secured during the 1996 September observing run. The positions of the nebular emission lines covered are indicated. The short-dashed line shows the 1 σ error applicable to each spectrum. The vertical long-dashed lines mark the locations of the strongest sky OH emission features; although they have been subtracted out, large residuals can remain if the skylines are saturated (see text).

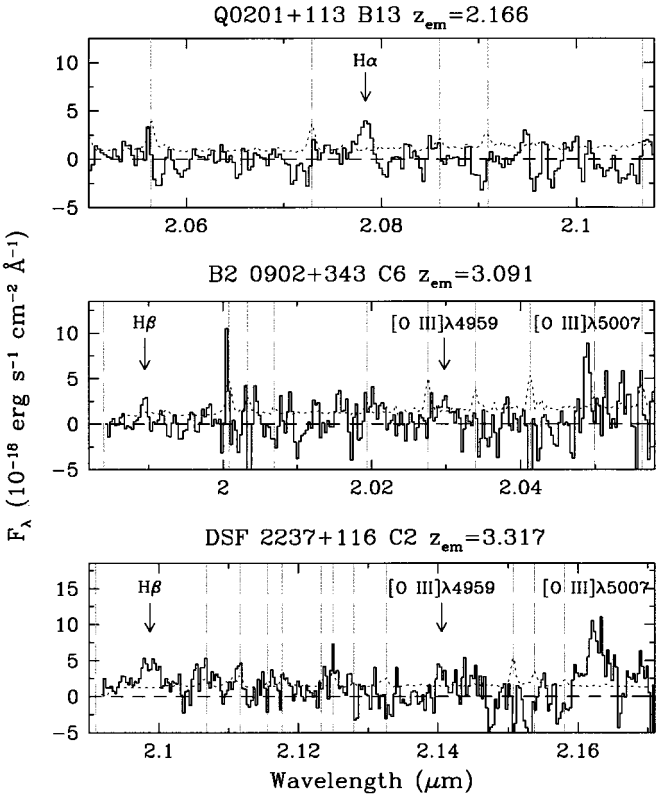

FIG. 3.—Same as for Fig. 2, showing the spectra recorded in the 1997 observing runs

two-dimensional images from the 1996 observations. In Table 2 we list the measured redshifts and fluxes of the nebular emission lines covered, together with the line luminosities deduced for $H_0 = 70$ km s^{-1} Mpc^{-1} and $q_0 = 0.1$ (we adopt these values throughout the paper). From the continuum fluxes implied by the K_{AB} mag (see Table 1), we calculate the values of rest-frame equivalent width listed in Table 2. It can be seen from the figures that, by targeting redshifts such that the nebular lines are well removed from the strongest night sky features, we have generally succeeded in detecting [O III] and Balmer emission lines from the H II regions of Lyman break galaxies at $z \simeq 3$.

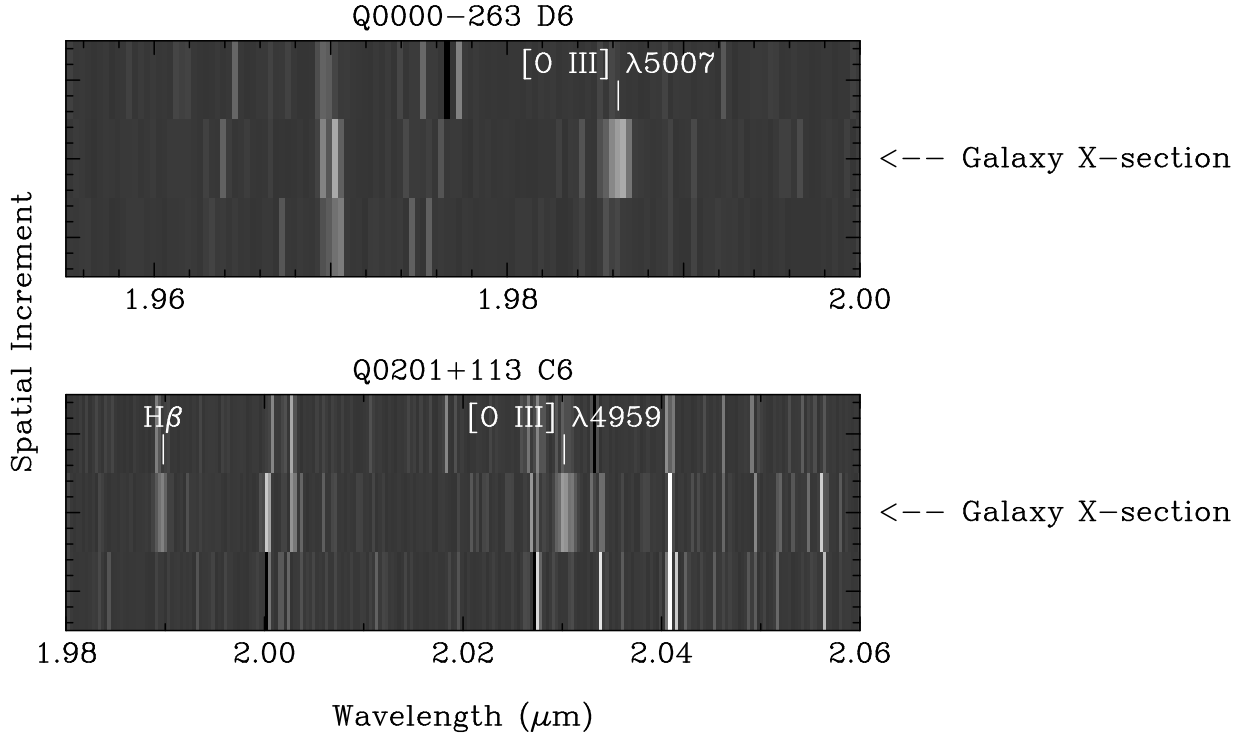

FIG. 4.—Portions of the coadded two-dimensional CGS4 images of Q0000−263 D6 and Q0201+113 C6. Each spatial increment is 1.″2 along the slit; the position of each galaxy on the slit was adjusted so that most of the light is in the central cross section. Most of the bright pixels are residuals from the subtraction of the strongest OH sky emission lines, the positions of which are indicated in Fig. 2.

TABLE 2

REDSHIFTS, FLUXES, LUMINOSITIES, AND EQUIVALENT WIDTHS OF NEBULAR EMISSION LINES

	Hβ λ4861.32				[O III] λ4958.91				[O III] λ5006.84				Hα λ6562.82			
NAME	z_{em}	F^a	L^b	$W_0{}^c$	z_{em}	F^a	L^b	$W_0{}^c$	z_{em}	F^a	L^b	$W_0{}^c$	z_{em}	F^a	L^b	$W_0{}^c$
Q0000−263 D6	...[d]	...[d]	...[d]	...[d]	...	≤2.5[e]	≤2[e]	≤23[e]	2.966	7.6 ± 0.7	6.1 ± 0.6	70 ± 6	...	...	...	...
Q0201+113 C6.....	3.094	2.6 ± 0.6	2.3 ± 0.5	53 ± 11	3.094	4.6 ± 0.9	4.0 ± 0.8	95 ± 20	...[f]	...[f]	...[f]	...[f]	...	...	...	...
Q0201+113 B13.....	...	...	...	...	...	...	...	...	...	...	...	...	2.166	6 ± 1	2.1 ± 0.4	72 ± 10
B2 0902+343 C6	3.091	3.0 ± 1	2.7 ± 0.8	40 ± 13	3.092	3.3 ± 1	3.0 ± 0.9	44 ± 13	3.091	7.7 ± 1.1	7.0 ± 1	102 ± 15	...	...	...	...
DSF 2237+116 C2.....	3.316	10 ± 2	11 ± 2	80 ± 13	...	≤7[e]	≤7[e]	≤55[e]	3.318	33 ± 5	37 ± 5	260 ± 40	...	...	...	...

NOTE.—Emission redshifts are vacuum heliocentric. 1 σ errors were measured from the error spectra shown in Figs. 2 and 3.

[a] Line flux in units of 10^{-17} ergs s^{-1} cm^{-2}.

[b] Line luminosity in units of 10^{42} ergs s^{-1} ($H_0 = 70$ km s^{-1}, $q_0 = 0.1$).

[c] Rest-frame equivalent width in Å.

[d] Outside the K-band.

[e] 3 σ limit.

[f] Blended with sky OH emission.

Even so, it is clear that the observations are at the limit of what can be achieved with 4 m class telescopes, resulting in detections at levels of only a few σ (see Table 2) despite the very long exposure times. In general, [O III] λ4959 is in the noise, but in each case the upper limit on its flux is consistent with the measured flux of λ5007, which is three times stronger. In one case, Q0201+113 C6, we do detect [O III] λ4959 but not λ5007, because at $z_{em} = 3.094$ the latter coincides with a strong OH line at 2.04993 μm, which is saturated in our spectra. In Q0000−263 D6, Hβ falls outside the K-band window.

Typical line fluxes are a few times 10^{-17} ergs s^{-1} cm^{-2}, approximately 1 order of magnitude lower than the limits achieved so far in wide-field surveys in the near infrared using narrowband imaging (e.g., Thompson, Mannucci, & Beckwith 1996). This is likely to be the reason why such surveys have not yet found a widespread population of star-forming galaxies at high redshift. Targeted searches for Hα emission at $z \simeq 2$ in QSO fields, using narrowband filters tuned to the redshifts of known absorbers, have been more successful (Teplitz, Malkan, & McLean 1998; Mannucci et al. 1998; Bechtold et al. 1998).

3. STAR FORMATION RATES AND DUST EXTINCTION

In Table 3 and Figure 5 we compare the values of the SFR deduced in the five galaxies from the measured luminosities in the Hβ line and in the far-UV continuum ($\lambda_0 =$ 1500 Å), respectively. At this stage we do *not* correct the observed fluxes for dust obscuration. In calculating SFR$_{H\beta}$, we have assumed a ratio Hα/Hβ = 2.75 (Osterbrock 1989) and Kennicutt's (1983) calibration SFR $= L_{H\alpha}/1.12 \times 10^{41}$ $M_\odot$ yr^{-1} (where $L_{H\alpha}$ is in ergs s^{-1}), which is appropriate for a Salpeter initial mass function (IMF) from $M = 100$–0.1 $M_\odot$.[7] For Q0000−263 D6, where only [O III] λ5007 is observed, we derive an upper limit to SFR$_{H\beta}$ assuming that λ5007/H$\beta \geq 2$. This is a conservative limit based on data from local star-forming regions (Terlevich et al. 1991; Stasinska & Leitherer 1996) as well as the three Lyman break galaxies in the present sample, where both [O III] and Hβ are detected (see Table 2).

[7] Madau et al. (1998) deduced a slightly different conversion factor, SFR $= L_{H\alpha}/1.58 \times 10^{41}$ $M_\odot$ yr^{-1}, using more recent population synthesis models. Adopting this calibration would *decrease* the values of SFR$_{H\beta}$ in col. (3) of Table 3 by 29%.

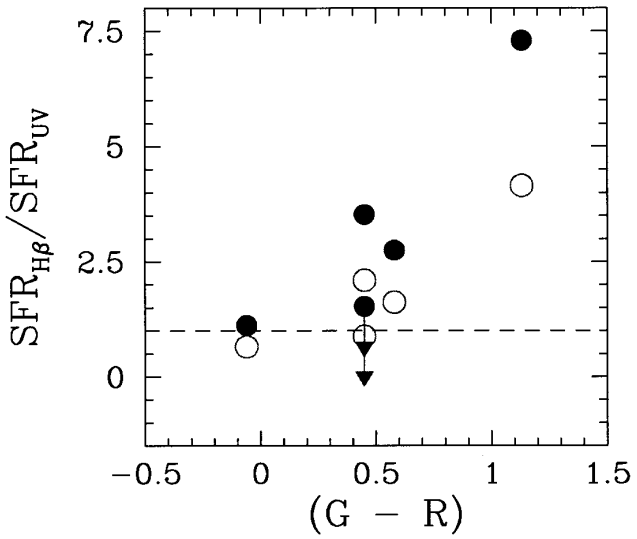

FIG. 5.—Ratio of the SFRs implied by the luminosities of the Hβ line and of the ultraviolet continuum, respectively, plotted as a function of the observed ($G-\mathscr{R}$) color (10^7 yr old continuous star formation model, *open circles*; 10^9 yr old continuous star formation model, *filled circles*). The horizontal dashed line is at SFR$_{H\beta}$ = SFR$_{UV}$.

Turning to the ultraviolet luminosity, it is important to realize that, although the continuum at 1500 Å is dominated by short-lived O and B stars, it does nevertheless show a modest increase with time in *continuous* star formation models. (In the case of an instantaneous burst of star formation, the ultraviolet luminosity obviously fades with time after the starburst.)[8] The Bruzual & Charlot (1996, private communication) models predict that, for a Salpeter IMF within the above limits and solar metallicity, the ultraviolet luminosity at 1500 Å from a region undergoing continuous star formation tends to an asymptote at 10^9 yr, at

[8] Throughout this paper we only consider "continuous" star formation models, in which gas is converted into stars at a constant rate, as opposed to "instantaneous burst" models, in which all stars are assumed to be formed at time $t = 0$, with negligible star formation thereafter. Clearly these are two limiting cases to the real star formation history of Lyman break galaxies. However, in our view single-burst models are less likely to apply to the galaxies observed here, because the Balmer and [O III] emission lines would fade rapidly after such a burst and would be undetectable at the sensitivity of the present observations after less than 10^7 yr (Stasinska & Leitherer 1996).

TABLE 3

STAR FORMATION RATES UNCORRECTED FOR DUST EXTINCTION

Name (1)	($G-\mathscr{R}$) (2)	SFR$_{H\beta}$ ($M_\odot$ yr^{-1})[a] (3)	SFR$_{UV7}$ ($M_\odot$ yr^{-1})[b] (4)	SFR$_{UV9}$ ($M_\odot$ yr^{-1})[c] (5)
Q0000−263 D6	0.45	≤75[d]	85	49
Q0201+113 C6.....	0.58	55	34	20
Q0201+113 B13.....	−0.06	19[e]	29	17
B2 0902+343 C6	0.45	67	32	19
DSF 2237+116 C2.....	1.13	270	65	37

[a] SFR deduced from the Hβ luminosity; typical error in the measured Hβ flux is ≤30% (see Table 2).

[b] SFR deduced from the continuum luminosity at 1500 Å adopting a 10^7 yr old continuous star formation model (see text for other assumptions).

[c] SFR deduced from the continuum luminosity at 1500 Å adopting a 10^9 yr old continuous star formation model.

[d] Assuming Hβ/λ5007 ≤ 0.5.

[e] Deduced directly from Hα.

TABLE 4

EXTINCTION AT 1500 Å DEDUCED BY COMPARING BALMER LINE AND ULTRAVIOLET CONTINUUM LUMINOSITIES

Name	$(G-\mathscr{R})$	$A_{\rm UV7}$[a]	$A_{\rm UV7}$[b]	$A_{\rm UV9}$[c]	$A_{\rm UV9}$[d]
Q0000−263 D6	0.45	≤ -0.19	≤ -0.26	≤ 0.64	≤ 0.90
Q0201+113 C6	0.58	0.72	1.02	1.51	2.14
Q0201+113 B13	−0.06	−0.63	−0.89	0.17	0.24
B2 0902+343 C6	0.45	1.10	1.56	1.88	2.67
DSF 2237+116 C2.....	1.13	2.13	3.01	2.97	4.20

[a] 10^7 yr old continuous star formation + SMC extinction curve.
[b] 10^7 yr old continuous star formation + Calzetti attenuation curve.
[c] 10^9 yr old continuous star formation + SMC extinction curve.
[d] 10^9 yr old continuous star formation + Calzetti attenuation curve.

which point a SFR $= 1\ M_\odot\ {\rm yr}^{-1}$ produces $L_{1500} = 10^{28}$ ergs s^{-1} Hz^{-1}. For comparison, 10^7 yr after the onset of star formation, the ultraviolet luminosity corresponding to SFR $= 1\ M_\odot\ {\rm yr}^{-1}$ is only $\sim$60% of the above value (see also Leitherer, Robert, & Heckman 1995). In the Bruzual & Charlot models these conversion factors do not depend sensitively on metallicity.[9]

At $z \simeq 3$ our $\mathscr{R}$ filter (with effective wavelength $\lambda = 6850$ Å) samples the rest-frame continuum near $\lambda_0 = 1710$ Å. Since our magnitudes are on the AB scale (AB $= -48.60 - 2.5 \log f_\nu$), the median $\mathscr{R} = 23.5$ of the Lyman break galaxies considered here corresponds to $f_\nu = 1.5 \times 10^{-29}$ ergs s^{-1} cm^{-2} Hz^{-1}; at $z = 3$ this in turn translates to a continuum luminosity $L_{1710} = 3.1 \times 10^{29}$ ergs s^{-1} Hz^{-1}. In arriving at the SFR listed in columns (4) and (5) of Table 3, we have applied small k-corrections (generally less than 10%), based on the spectral slopes measured from our Keck LRIS spectra, to deduce L_{1500} from the values of L_{1710} implied by the galaxy R mag.

There are two conclusions that can be drawn from the results in Table 3. First, in most cases the Balmer lines indicate SFRs that broadly agree, to within factors of 2–3, with the values obtained by applying the Bruzual & Charlot (1996, private communication) models to the observed ultraviolet continuum luminosities. This is the level of agreement to be expected between different star formation indicators, even in the local universe (e.g., Meurer et al. 1995), given the systematic uncertainties in the calibrations and the possibility that ionized gas and early-type stars have different spatial distributions (e.g., Leitherer et al. 1996).

Second, Figure 5 suggests that there may be a trend between the $(G-\mathscr{R})$ color and ${\rm SFR}_{\rm H\beta}/{\rm SFR}_{\rm UV}$ in the sense that the redder galaxies have apparently the larger values of this ratio. Thus Q0201+113 B13, which is among the bluest galaxies in our entire sample, has a Balmer line flux close to that predicted from its ultraviolet continuum luminosity, while in DSF 2237+116 C2, which with $(G-\mathscr{R}) = 1.13$ is close to the red limit of our selection criteria for Lyman break galaxies, we apparently see 4–7 times more Hβ photons than expected. The other three galaxies are intermediate cases. Before reading too much into this "trend," we must remember that we are dealing with only a small number of measurements from infrared spectra of low S/N. Nevertheless, the effect is in the direction expected from dust extinction, which is more effective at ultraviolet wavelengths than in the optical. It is worthwhile considering, then, the magnitude of the ultraviolet extinction at 1500 Å, A_{1500}, implied by the ${\rm SFR}_{\rm H\beta}/{\rm SFR}_{\rm UV}$ ratios and how this is related to the observed $(G-\mathscr{R})$ colors.

3.1. *Ultraviolet Extinction of Lyman Break Galaxies*

Specifically, we are going to determine the values of A_{1500} that satisfy the requirement ${\rm SFR}'_{\rm UV} = {\rm SFR}'_{\rm H\beta}$, where SFR$'$ are the SFRs corrected for extinction. This would be a straightforward calculation were it not for the fact that we are totally ignorant of the wavelength dependence of dust extinction in Lyman break galaxies! Here we consider what are generally thought to be two limiting cases, the extinction curve determined for stars in the Small Magellanic Cloud (Bouchet et al. 1985; Gordon & Clayton 1998) and the "attenuation" curve derived from the integrated spectra of local star-forming galaxies (Calzetti, Kinney, & Storchi-Bergmann 1994; Calzetti 1997a). The former rises steeply toward shorter wavelengths, while the latter is "grayer" (see, for example, Fig. 2*a* of Calzetti 1997a). These differences are thought to arise, at least in part, from different geometrical configurations of the dust and background sources of light. The SMC extinction curve is derived from observations of individual stars, where dust is mostly in a foreground screen that removes both scattering and absorption components of the extinction curve, whereas the integrated stellar spectrum that emerges from an extended region presumably includes photons scattered *into* the line of sight by dust mixed with the stars. Whether the latter situation also applies to Lyman break galaxies depends to some extent on the geometrical configuration of the large-scale outflows that seem to be a common feature of their interstellar media (see § 5).

For the Bouchet et al. (1995) SMC reddening law with Pei's (1992) normalization,

$$A_{1500} = 3.44 \times \log\,({\rm SFR}_{\rm H\beta}/{\rm SFR}_{\rm UV})\,, \qquad (1)$$

where A_{1500} is in mag, whereas the Calzetti (1997a) attenuation curve gives

$$A_{1500} = 4.87 \times \log\,({\rm SFR}_{\rm H\beta}/{\rm SFR}_{\rm UV})\,. \qquad (2)$$

With these conversion factors we deduce the values of A_{1500} listed in Table 4. It can be readily seen that the uncertainties in the conversion from L_{1500} to SFR and in the wavelength dependence of the extinction combine to give a wide range of possibilities for A_{1500}. Ultraviolet extinctions by $\approx$1–2 mag seem typical, but we also find some unlikely solutions. The large dust corrections indicated for DSF 2237+116 C2, if the Calzetti reddening curve applies, would imply SFRs in excess of 1000 $M_\odot\ {\rm yr}^{-1}$. We have retained negative (and

[9] An empirical determination of the metallicity dependence of the integrated ultraviolet continuum of stellar populations awaits the availability of the appropriate stellar libraries.

TABLE 5

EXTINCTION AT 1500 Å DEDUCED FROM THE SLOPE OF THE ULTRAVIOLET CONTINUUM

Name (1)	$(G-\mathscr{R})$ (2)	β[a] (3)	$E(G-\mathscr{R})$[b] (4)	A_{UV7}[c] (5)	A_{UV7}[d] (6)	$E(G-\mathscr{R})$[e] (7)	A_{UV9}[f] (8)	A_{UV9}[g] (9)
Q0000−263 D6	0.45	−1.1	0.41	0.80	2.13	0.26	0.50	1.33
Q0201+113 C6.....	0.58	−1.2	0.43	0.72	1.77	0.22	0.36	0.88
Q0201+113 B13.....	−0.06	−2.2	0.04	0.11	0.23	−0.09	−0.27	−0.53
B2 0902+343 C6	0.45	−1.5	0.27	0.44	1.08	0.05	0.09	0.21
DSF 2237+116 C2.....	1.13	−0.4	0.71	1.14	2.44	0.46	0.75	1.58

[a] Spectral slope of the ultraviolet continuum ($F_\lambda \propto \lambda^\beta$) after correction for Lyα forest opacity.
[b] Excess over the color predicted by the model SED for a 10^7 yr old continuous star formation and Lyα forest opacity.
[c] 10^7 yr old continuous star formation + SMC extinction curve.
[d] 10^7 yr old continuous star formation + Calzetti attenuation curve.
[e] Excess over the color predicted by the model SED for a 10^9 yr old continuous star formation and Lyα forest opacity.
[f] 10^9 yr old continuous star formation + SMC extinction curve.
[g] 10^9 yr old continuous star formation + Calzetti attenuation curve.

therefore unphysical) values of A_{1500} in Table 4, because they give an indication of the inherent limitations of the analysis, which forces $SFR'_{UV} = SFR'_{H\beta}$. Other possibilities are that our assumption that $\lambda5007/H\beta \geq 2$ in Q0000−263 D6 is incorrect and that in Q0201+113 B13 the Balmer lines suffer higher extinction than the stellar continuum (or some of the ionizing photons escape the nebula). Note that the combination of the 10^9 yr old continuous star formation model, which gives the lower SFR for a given ultraviolet luminosity, and the Calzetti attenuation, which has the lower differential extinction between 1500 Å and Hβ, is the one that produces the largest values of A_{1500}.

3.1.1. *Extinction Estimates from the Slope of the Ultraviolet Continuum*

With a larger sample of emission line measurements, it will be possible in future to obtain an independent estimate of the SFR density at high z that is less sensitive to dust corrections than the current rest-frame ultraviolet data. For the moment, however, it is of interest to consider whether the few Balmer line detections available can be used to "calibrate," as it were, a dust extinction index based on the ultraviolet SED, given the large number of ultraviolet spectra of Lyman break galaxies now being obtained (Steidel et al. 1998b).

An index often used is β, the slope of the ultraviolet continuum approximated by a power law of the form $F_\lambda \propto \lambda^\beta$. Model SEDs (e.g., Leitherer & Heckman 1995) show that β changes relatively little with age and metallicity; for a Salpeter IMF from $M = 100$–$0.1\ M_\odot$, the Bruzual & Charlot (1996, private communication) continuous star formation models have β increasing from ~ -2.5 to ~ -2 over the period 10^7–10^9 yr. Empirically, the measured values of β correlate with both the far-infrared excess (Meurer et al. 1995) and the reddening deduced from the Balmer decrement (Calzetti 1997a), although there is considerable scatter in these relations. The empirical starburst template spectrum derived by Calzetti (1997b) has $\beta = -2.1$, which would suggest that the youngest model SEDs may be too blue.

At $z \simeq 3$ our $(G-\mathscr{R})$ color provides a more reliable estimate of the continuum slope between 1190 and 1710 Å (the effective wavelengths of the two filters are 4740 and 6850 Å, respectively) than the value that could be measured directly from the Keck spectra. The reason for this is that the spectra are obtained through multiobject apertures that have fixed orientation on the sky; differential atmospheric refraction can lead to increasing light losses with decreasing wavelength, which may be difficult to calibrate out. The net effect is to artificially redden the spectra (by an unknown amount), and it is therefore dangerous to use published Keck LRIS spectra to measure β.

For comparison with other analyses, we have listed in column (3) of Table 5 the values of β implied by the observed $(G-\mathscr{R})$ color for each of the five galaxies in the present sample. They were calculated by convolving power laws in F_λ with the G and $\mathscr{R}$ filter transmission curves and folding in the average Lyα forest opacity as a function of redshift according to the prescription by Madau (1995).[10]

In order to estimate the dust reddening of the ultraviolet continuum, we have determined a color excess $E(G-\mathscr{R}) = (G-\mathscr{R})_{obs} - (G-\mathscr{R})_{calc}$, where the two terms on the right-hand side of the equality are the observed and expected values of $(G-\mathscr{R})$. Again, we have calculated $(G-\mathscr{R})_{calc}$ by convolving the appropriately redshifted Bruzual & Charlot (1996, private communication) model SEDs with the filter transmission curves and allowing for the Lyα forest opacity. The resulting values of $E(G-\mathscr{R})$ for the 10^7 and 10^9 yr model SEDs are listed in columns (4) and (7) of Table 5, respectively. Columns (5)–(6) and (8)–(9) of Table 5 then give the values of A_{1500} implied by the $(G-\mathscr{R})$ color excess, depending on whether the SMC or Calzetti extinction law is adopted. Once again we see that A_{1500} is not well constrained, the different permutations of intrinsic ultraviolet slope and reddening curve allowing solutions that span a $1-1.5$ mag range. In this case it is the combination of the Calzetti curve and 10^7 yr model (with its very blue intrinsic slope) that requires the largest values of ultraviolet extinction.

We can proceed further, however, by considering which set of model assumptions results in the values of A_{1500} for each galaxy that are most consistent between Tables 4 and 5. Comparing the entries in the two tables, we see that for Q0000−263 D6 the combination of 10^9 yr SED (UV9) and SMC extinction law satisfies both the ultraviolet slope and the $SFR_{H\beta}/SFR_{UV}$ tests with $A_{1500} \simeq 0.5$. UV7 + SMC gives a good solution in Q0201+113 C6 for $A_{1500} \simeq 0.7$. The agreement is less than optimum in B2 0902+343 C6

[10] Along any particular sight line, the Lyα forest opacity may differ somewhat from Madau's average. However, the ensuing error in slope of the ultraviolet continuum is small compared with that which could result from the uncertain photometric calibration of the LRIS spectra.

TABLE 6

VELOCITY DISPERSIONS AND VIRIAL MASSES

Name (1)	σ (km s^{-1}) (2)	Half-light radius (arcsec) (3)	Half-light radius (kpc)[a] (4)	M_{vir} (10^{10} $M_\odot$) (5)
Q0000−263 D6	60 ± 10	0.22[b]	1.8	0.8
Q0201+113 C6	70 ± 20	0.25[b]	2.0	1.2
Q0201+113 B13.....	85 ± 15	0.2[c]	1.5	1.3
B2 0902+343 C6	55 ± 15	...	...	...
DSF 2237+116 C2.....	190 ± 25	0.2[c]	1.5	5.5

[a] $H_0 = 70$ km s^{-1}; $q_0 = 0.1$.
[b] From *HST* NICMOS images (Giavalisco et al. 1999).
[c] From Keck II NIRC images.

and DSF 2237+116 C2, but even here we see that the UV7 SED gives answers that differ by only ≈0.5 mag between Tables 4 and 5 independently of the extinction curve used. Q0201+113 B13 is not useful in this context, because its spectrum is essentially unreddened.

It would be inappropriate to take these comparisons too literally and, for example, conclude that a particular extinction law is favored or deduce an age for the star-forming galaxies. The reasons are that our infrared spectra are of low S/N and the galaxies probed are not sufficiently reddened to discriminate positively between the models. Furthermore, we do not even know at this stage that the models are internally consistent. For instance, the Bruzual & Charlot (1996, private communication) SED for the 10^7 yr old continuous star formation case may have an ultraviolet slope that is too blue compared to the unreddened continuum of the typical Lyman break galaxy and yet provides the correct calibration of the luminosity at 1500 Å as a function of SFR: the slope and normalization of the models are independent parameters to some extent.

What seems to emerge from the comparison of Tables 4 and 5, however, is that the values of A_{1500} that fit best both the ultraviolet slopes and the ratios of the Balmer lines to the ultraviolet luminosity are in every case *intermediate* between the extreme possibilities allowed by the different models. Very high and very low values of ultraviolet extinction seem to be excluded even by the present limited sample.

4. LINE WIDTHS AND MASSES OF LYMAN BREAK GALAXIES

In column (2) of Table 6, we have listed the values of the velocity dispersion σ (=FWHM/2.355) deduced by fitting the Balmer and [O III] emission lines with Gaussian profiles and correcting for the instrumental resolution (thermal motions make a very small contribution to the line widths found here). In general, there is good agreement between values of σ measured from different emission lines in the same galaxy; the errors quoted in Table 6 were obtained by propagating the error of each Gaussian fit. We find that four out of the five galaxies have similar velocity dispersions, $\sigma \simeq (60\text{–}80)$ km s^{-1}, while in the fifth, DSF 2237+116 C2, the lines are apparently about three times wider.

HST NICMOS images of two of the galaxies in our sample (see Table 6) show well-resolved objects with half-light radii $r \sim 0.25''$ (corresponding to ≈2 kpc at $z \simeq 3$ in the cosmology adopted here). For two other galaxies, we measure similar sizes from near-IR images obtained in 0.″5 seeing with NIRC on the Keck II telescope (when both are available, ground-based and *HST* measurements are in good agreement). Combining these radii with the measured velocity dispersions, we obtain virial masses $M_{vir} \approx (1\text{–}5) \times 10^{10}\ M_\odot$ (see col. [5] of Table 6). Thus, in Lyman break galaxies at $z \simeq 3$ we already find masses comparable to, or exceeding, that of the Milky Way bulge (Dwek et al. 1995). In reality, we may well be underestimating the total masses of these systems, because at the low S/N of our observations we could easily miss broader components of the emission lines.[11] As discussed by Steidel et al. (1998a; see also Giavalisco et al. 1998; Adelberger et al. 1998), the clustering properties of Lyman break galaxies, interpreted within the cold dark matter scenario of galaxy formation, point to dark halo masses $M_{DM} \gtrsim 10^{11}\ M_\odot$.

If star formation takes place in rotationally supported disks, the typical $\sigma \simeq 70$ km s^{-1} implies rotational velocities $v_{rot} \simeq 120$ km s^{-1} (Rix et al. 1997). However, it has been known for a long time that in local starburst galaxies the nuclear emission lines do not reflect the full rotation speed of the galaxy (Weedman 1983). Lehnert & Heckman (1996) found that starbursts are roughly confined to the solid-body part of the galaxy rotation curve and that the widths of the emission lines typically underestimate the full v_{rot} by a factor of ≈2. If a similar situation applies to galaxies at $z \simeq 3$ (a highly speculative hypothesis, admittedly), rotational velocities $v_{rot} \approx 200\text{–}250$ km s^{-1} may be indicated. Note that in this picture, where the emission in the nebular lines is dominated by H II regions in the star-forming cores of larger galaxies, it is reasonable to expect the strong, saturated interstellar absorption lines to be broader than Hβ and [O III], as is indeed the case (Steidel et al. 1996), because the absorption takes place over longer path lengths, presumably through half of the galaxy. In this case *both* galactic rotation and the large-scale "stirring" of the interstellar gas by supernovae and stellar winds (see § 5) may be contributing to the strengths of the absorption lines. Heckman (1998) reached a similar conclusion for local starburst galaxies.

5. REDSHIFTS OF EMISSION LINES AND LARGE-SCALE MOTIONS

Table 7 lists the relative velocities of the interstellar absorption, nebular emission, and Lyα emission lines; we have *assumed* that the Balmer and [O III] emission lines are

[11] It is also conceivable that we may *over*estimating the virial masses if the emission line widths have significant contributions from gas accelerated to high velocities from supernova explosions and stellar winds.

TABLE 7

RELATIVE VELOCITIES OF INTERSTELLAR ABSORPTION, NEBULAR EMISSION, AND Lyα EMISSION LINES

Name	$V_{\rm ISabs}$ (km s^{-1})	$V_{\rm H\,II}$ (km s^{-1})	$V_{\rm Ly\alpha}$ (km s^{-1})
Q0000−263 D6	-435 ± 50[a]	0	+375
Q0201+113 C6.....	-3020 ± 30	0	...
Q0201+113 B13.....	+250	0	...
B2 0902+343 C6	-800 ± 300	0	+575
DSF 2237+116 C2.....	$+110 \pm 60$	0	+1090

[a] The errors quoted are the standard deviation of different interstellar absorption lines.

at the systemic redshift of each galaxy. The immediate conclusion is that large velocity fields are a common feature of Lyman break galaxies, confirming the initial hints provided by the large equivalent widths of the interstellar absorption lines (Steidel et al. 1996) and in agreement with the analyses by Lowenthal et al. (1997) and Franx et al. (1997). In all three cases where we detect Lyα emission, the line peak is *redshifted* by $\approx$1000 km s^{-1} relative to the metal absorption lines. In two out of three cases (Q0000−263 D6 and B2 0902+343 C6), Hβ and [O III] are at intermediate velocities; furthermore, in Q0000−263 D6, Lyα emission exhibits an obvious P-Cygni profile, with a sharp drop on the blue side and a long tail of emission extending to $\sim +1100$ km s^{-1} on the relative velocity scale of Table 7 (see Fig. 8 of Pettini et al. 1998).

These characteristics are most easily interpreted as evidence for large-scale outflows with velocities of $\gtrsim$500 km s^{-1} in the interstellar media of the galaxies observed. In this picture Lyα emission is suppressed by resonant scattering, and the only Lyα photons that can escape unabsorbed in our direction are those back-scattered from the far side of the expanding nebula, whereas in absorption against the stellar continuum we see the approaching part of the outflow. The data also show that the real situation is probably more complex than this simple sketch. In one case, DSF 2237+116 C2, Hβ and [O III] emission are apparently at roughly the same velocity as the absorption lines, even though Lyα emission is redshifted by $\approx$1000 km s^{-1}. Most difficult to understand is the 3200 km s^{-1} difference between emission and absorption lines in Q0201+113 C6, large enough to raise the question of whether the two sets of lines are at all related!

Nevertheless, all of the above features—blueshifted metal lines, redshifted Lyα emission, and a variety of Lyα profiles ranging from emission to P-Cygni and to damped absorption—have been observed in *HST* spectra of nearby H II and starburst galaxies (Kunth et al 1998; González Delgado et al. 1998), although lower outflows velocities are normally involved. The variety of Lyα emission-absorption profiles may reflect different stages in the interaction of the mechanical energy generated by the starburst with the interstellar medium of the host galaxy and/or different viewing angles (Giavalisco, Koratkar, & Calzetti 1996). Irrespective of the details of this picture, two facts are clear. First, we see *directly* the process by which heavy elements can be distributed far from the sites of production (Heckman 1998). If outflows of $\sim$500 km s^{-1} are maintained over lifetimes of $\gtrsim 1 \times 10^8$ yr, the metals will travel over distances $\gtrsim$50 kpc, more than enough to seed the entire dark matter halo of each Lyman break galaxy. Second, just as the luminosity of Lyα emission is in general poorly related to the SFR, its wavelength is not a useful measure of the galaxy systemic redshift.

6. DISCUSSION

Our first detections of nebular emission lines at $z \simeq 3$ have predictably gone only partway toward determining the typical extinction suffered by the ultraviolet continuum of Lyman break galaxies. The present sample of five galaxies includes one that is essentially unreddened, three where the continuum at 1500 Å is dimmed by between $\sim$0.5 and $\sim$1 mag, and one where the extinction may be as much as $\sim$2.5 mag. The main conclusion reached in § 3, however, is that the values of A_{1500} that best fit all the available data are intermediate solutions within the wide range allowed by different combinations of SEDs and reddening curves.

Recently, Dickinson (1998) has analyzed the $(G-\mathscr{R})$ colors of our entire sample of more than 400 spectroscopically confirmed Lyman break galaxies in the same way as discussed in § 3.1.1 above. His analysis showed that, based on the ultraviolet slope alone, the value of A_{1500} to be applied to the population as a whole can be as little as 0.75 mag or as large as 3.1 mag for the different combinations of SEDs and extinction curves considered in § 3.1.1. The upper end of this range agrees with the factor of 16 proposed by Sawicki & Yee (1998); in both cases, such high values are derived assuming the bluest intrinsic continuum (UV7 in the notation above) and the grayest extinction curve (Calzetti 1997a).

If our preliminary conclusion for the five galaxies considered here applies to the whole population, it would favor values of A_{1500} near the middle of the range determined by Dickinson (1998); thus, $A_{1500} \simeq$ 1–2 may be the typical ultraviolet extinction (in mag) suffered by Lyman break galaxies at 1500 Å. If this still-tentative statement holds up in the light of future infrared observations, several interesting consequences follow.

First, this amount of dust would produce an extinction $A_{2800} \simeq$ 0.5–1.5 mag (SMC and Calzetti curves, respectively) of the *near*-UV continuum of galaxies at $z \lesssim 1$ in the Canada-France Redshift Survey (Lilly et al. 1996). This is in good agreement with available determinations of A_{2800}, based on the comparison between the luminosities in Hα and in the continuum at 2800 Å (Tresse & Maddox 1998; Glazebrook et al. 1999; see also Flores et al. 1998). Similarly, Buat & Burgarella (1998) recently concluded that $A_{2000} \simeq 1.2$ mag is typical of nearby starburst galaxies. Thus there is no need to assume that, as we look back to earlier epochs, an increasing fraction of the star formation activity takes place in highly obscured galaxies (such a scenario would be called for if the far-UV continuum of Lyman break galaxies were suppressed by more than a factor of 10; Madau et al. 1998; Guiderdoni et al. 1997). The dust corrections proposed here, while raising the values of the ultraviolet luminosity density by larger factors at $z > 3$ than at $z < 1$, still maintain the same broad picture of the cosmic star formation history sketched by Madau et al. (1996), with the peak in activity at an intermediate epoch between these two redshifts.

(Of course the present data do not address the separate question of whether our photometric selection based on the Lyman break misses a significant component of the galaxy population at $z \simeq 3$, in which the ultraviolet continuum may be too faint to be detected. However, as discussed by

Adelberger et al. (1998), the clustering properties of the Lyman break galaxies suggest that such an unseen population is likely to contribute only a small fraction of the total number of *luminous* galaxies at these redshifts.)

Second, it is of interest to ask where the metals associated with the higher, dust-corrected rates of star formation are to be found. Pettini et al. (1997) showed that at $z \gtrsim 2$, damped Lyα systems can account for the metal production expected from the *uncorrected* ultraviolet luminosity. We note, however, that the estimates of metallicity by Pettini et al. (1997) are based on measurements of the abundance of Zn, which traces that of the Fe-peak elements. The average metallicity of damped Lyα absorbers (DLAs), $Z_{\rm DLA}$, may need to be corrected upward by a factor of ≈ 2 if O and other α elements are overabundant by 0.4 dex relative to Fe, as is the case in metal-poor stars of the Milky Way (e.g., McWilliam 1997). Therefore, even when dust obscuration is taken into account, there may still be a broad consistency, given the uncertainties, between these two independent measures of the metallicity of the universe—the metals seen in absorption toward distant QSOs and those produced by the star-forming galaxies imaged directly. On the other hand, if future observations were to reveal that we have underestimated the dust correction to the ultraviolet luminosity of $z \simeq 3$ galaxies, the implication would be that DLA systems "miss" metal-rich regions of the universe, either because current QSO absorption-line samples are biased in favor of metal- and dust-poor sight lines and/or because the metals may be retained close to their production sites. It will be possible to test these ideas in the near future as wide-field surveys yield new and larger samples of damped Lyα systems toward fainter—and potentially more reddened—QSOs than studied up to now (e.g., Shaver et al. 1998).

7. SUMMARY

The main results of this work are as follows:

1. We report the first detections of Balmer and [O III] emission lines from five Lyman break galaxies at $z \simeq 3$, achieved by targeting redshifts such that these transitions fall in the gaps between the strong OH lines that dominate the near-infrared sky. The five galaxies span nearly the full range of our color selection criteria for Lyman break galaxies.

2. For a Salpeter IMF between 100 and 0.1 $M_\odot$, neglecting dust extinction, the measured Hβ luminosities of $\sim(0.8$–$10) \times 10^{42}$ ergs s^{-1} ($H_0 = 70$ km s^{-1} Mpc^{-1}, $q_0 = 0.1$) imply SFRs of between ~ 20 and ~ 270 $M_\odot$ yr^{-1}. These values are generally larger than those estimated from the ultraviolet continuum at 1500 Å by factors of between ~ 0.7 and ~ 7.

3. The present sample is too small to determine reliably the value of A_{1500}, the dust extinction suffered by the continuum at 1500 Å, given the uncertainties in the model SEDs and in the wavelength dependence of the extinction curve. However, in general, we find that the solutions that best fitted *both* the slope and the luminosity of the ultraviolet continuum (relative to Hβ) correspond to intermediate values of extinction within the large range allowed by the models. Thus, we favor $A_{1500} \simeq 1$–2 mag as the values most likely to be representative of the whole sample of Lyman break galaxies.

4. The amount of dust implied would depress the *near*-UV continuum by only $A_{2800} \simeq 0.5$–1.5 mag, in good agreement with recent determinations of this quantity for *CFRS* galaxies at $z < 1$. The upward corrections proposed do not require a significant revision of the broad picture of the star formation history of the universe put together by Madau et al. (1996). Similarly, there is still a plausible agreement between the metal production associated with the star-forming galaxies we see and the heavy elements detected in absorption against distant QSOs.

5. The nebular emission lines recorded are resolved in every case. It appears that the typical velocity dispersion is $\sigma \simeq 70$ km s^{-1}, although we also find one galaxy where the line widths are nearly three times larger. With typical half-light radii of ~ 2 kpc, virial masses $M_{\rm vir} \approx (1 - 5) \times 10^{10}$ $M_\odot$ are suggested. It is possible that both velocities and masses have been underestimated, because with the limited sensitivity of the present observations we may well be seeing only the inner cores of the galaxies, where star formation is most in evidence.

6. The relative redshifts of the interstellar absorption, nebular emission, and Lyα emission lines indicate that large-scale outflows with velocities of at least ≈ 500 km s^{-1} are a common feature of the interstellar media of Lyman break galaxies. These outflows, presumably driven by the mechanical energy generated in the star formation episodes, can distribute the products of stellar nucleosynthesis over large volumes.

7. Perhaps the most valuable aspect of this work is in showing that infrared spectroscopy of galaxies at $z \simeq 3$ is feasible and in highlighting the wealth of information that such spectra potentially offer. With the forthcoming availability of medium-resolution spectrographs on large telescopes, we expect that infrared observations will play a major role in advancing our understanding of the nature of Lyman break galaxies.

We are grateful to the UKIRT time assignment committee for their continuing support of this work, and to the staff at UKIRT and at the Joint Astronomy Center in Hilo for their generous and competent assistance with the observations. The interpretation of these results has benefited much from discussions with many colleagues, in particular, Daniela Calzetti, Karl Glazebrook, Tim Heckman, Claus Leitherer, Piero Madau, Gerhardt Meurer, and Roberto Terlevich. We are grateful to the referee, Arjun Dey, for constructive comments that improved the paper. C. C. S. acknowledges support from the National Science Foundation through grant AST 94-57446 and from the Alfred P. Sloan Foundation. M. G. has been supported through grant HF-01071.01-94A from the Space Telescope Science Institute, which is operated by the Association of Universities for Research in Astronomy, Inc., under NASA contract NAS 5-26555.

REFERENCES

Adelberger, K. L., Steidel, C. C., Giavalisco, M., Dickinson, M., Pettini, M., & Kellogg, M. 1998, ApJ, 505, 18
Bechtold, J., Elston, R., Yee, H. K. C., Ellingson, E., & Cutri, R. M. 1998, in The Young Universe: Galaxy Formation and Evolution at Intermediate and High Redshift (San Francisco: ASP), 241
Blain, A. W., Smail, I., Ivison, R. J., & Kneib, J.-P. 1998, MNRAS, submitted (astro-ph/9806062)
Bouchet, P., Lequeux, J., Maurice, E., Prevot, L., & Prevot-Burnichon, M. L. 1985, A&A, 149, 330
Buat, V., & Burgarella, D. 1998, A&A, 334, 772
Calzetti, D. 1997a, in AIP Conf. Proc. 408, The Ultraviolet Universe at at Low and High Redshift: Probing the Progress of Galaxy Evolution, ed. W. H. Waller, M. N. Fanelli, J. E. Hollis, & A. C. Danks (New York: Woodbury), 403
———. 1997b, AJ, 113, 162
Calzetti, D., Kinney, A. L., & Storchi-Bergmann, T. 1994, ApJ, 429, 582
Dickinson, M. 1998, in STScI Symp. Ser., The Hubble Deep Field, ed. M. Livio, S. M. Fall, & P. Madau, in press (astro-ph/9802064)
Dwek, E., et al. 1995, ApJ, 445, 716
Eales, S. A., & Rawlings, S. 1993, ApJ, 411, 67
Flores, H., et al. 1998, A&A, submitted
Franx, M., Illingworth, G., Kelson, D., van Dokkum, P., & Tran, K.-V. 1997, ApJ, 486, L75
Giavalisco, M., Koratkar, A., & Calzetti, D. 1996, ApJ, 466, 831
Giavalisco, M., Steidel, C. C., Adelberger, K. L., Dickinson, M. E., Pettini, M., & Kellogg, M. 1998a, ApJ, 503, 543
Giavalisco, M., et al. 1999, in preparation
Glazebrook, K., Blake, C., Economou, F., Lilly, S., & Colless, M. 1999, MNRAS, in press (astro-ph/9808276)
González Delgado, R. M., Leitherer, C., Heckman, T., Lowenthal, J. D., Ferguson, H. C., & Robert, C. 1998, ApJ, 495, 698
Gordon, K. D., & Clayton, G. C. 1998, ApJ, 500, 816
Guiderdoni, B., Bouchet, F., Puget, J. L., Lagache, G., & Hivon, E. 1997, Nature, 390, 257
Heckman, T. M. 1998, in The Most Distant Radio Galaxies, ed. P. Best, H. Rottgering, & M. Lehnert (Dordrecht: Reidel), in press (astro-ph/9801155)
Kennicutt, R. 1983, ApJ, 272, 54
Kunth, D., Mas-Hesse, J. M., Terlevich, E., Terlevich, R., Lequeux, J., & Fall, S. M. 1998, A&A, 334, 11
Lehnert, M. D., & Heckman, T. M. 1996, ApJ, 472, 546
Leitherer, C., & Heckman, T. M. 1995, ApJS, 96, 9
Leitherer, C., Robert, C., & Heckman, T. M. 1995, ApJS, 99, 173
Leitherer, C., Vacca, W. D., Conti, P. S., Filippenko, A. V., Robert, C., & Sargent, W. L. W. 1996, ApJ, 465, 717
Lilly, S. J., Le Févre, O., Hammer, F., & Crampton, D. 1996, ApJ, 460, L1
Lowenthal, J., et al. 1997, ApJ, 481, 673
Madau, P. 1995, ApJ, 441, 18
Madau, P., Ferguson, H. C., Dickinson, M. E., Giavalisco, M., Steidel, C. C., & Fruchter, A. 1996, MNRAS, 283, 1388
Madau, P., Pozzetti, L., & Dickinson, M. 1998, ApJ, 498, 106
Mannucci, F., Thompson, D., Beckwith, S. V. W., & Williger, G. M. 1998, ApJ, 501, L11
McWilliam, A. 1997, ARA&A, 35, 503
Meurer, G. R., Heckman, T. M., Lehnert, M. D., Leitherer, C., & Lowenthal, J. 1997, AJ, 114, 54
Meurer, G. R., Heckman, T. M., Leitherer, C., Kinney, A., Robert, C., & Garnett, D. R. 1995, AJ, 110, 2665
Mushotzky, R. F., & Loewenstein, M. 1997, ApJ, 481, L63
Osterbrock, D. E. 1989, Astrophysics of Gaseous Nebulae and Active Galactic Nuclei (Mill Valley: University Science Books)
Pei, Y. C. 1992, ApJ, 395, 130
Pettini, M., Smith, L. J., King, D. L., & Hunstead, R. W. 1997, ApJ, 486, 665
Pettini, M., Steidel, C. C., Adelberger, K. L., Kellogg, M., Dickinson, M., & Giavalisco, M. 1998, in Cosmic Origins, ed. C. E. Woodward, J. M. Shull, & H. A. Thronson (San Francisco: ASP), 67
Ramsay, S. K., Mountain, C. M., & Geballe, T. R. 1992, MNRAS, 259, 751
Renzini, A. 1997, ApJ, 488, 35
Rix, H. W., Guhathakurta, P., Colless, M., & Ing, K. 1997, MNRAS, 285, 779
Sawicki, M., & Yee, H. K. C. 1998, AJ, 115, 1329
Shaver, P. A., Hook, I. M., Jackson, C. A., Wall, J. V., & Kellermann, K. I. 1998, in Highly Redshifted Radio Lines, ed. C. Carilli, S. Radford, K. Menten, & G. Langston (San Francisco: ASP), in press (astro-ph/9801213)
Stasinska, G., & Leitherer, C. 1996, ApJS, 107, 661
Steidel, C. C., Adelberger, K. L., Dickinson, M., Giavalisco, M., Pettini, M., & Kellogg, M. 1998a, ApJ, 492, 428
———. 1998b, Philos. Trans. R. Soc. London, A., in press (astro-ph/9805267)
Steidel, C. C., Giavalisco, M., Pettini, M., Dickinson, M., & Adelberger, K. L. 1996, ApJ, 462, L17
Steidel, C. C., Pettini, M., & Hamilton, D. 1995, AJ, 110, 2519
Teplitz, H., Malkan, M., & McLean, I. S. 1998, ApJ, 506, 519
Terlevich, R., Melnick, J., Masegosa, J., Moles, M., & Copetti, M. V. F. 1991, A&AS, 91, 285
Thompson, D., Mannucci, F., & Beckwith, S. V. W. 1996, AJ, 112, 1794
Trager, S. C., Faber, S. M., Dressler, A., & Oemler, A. 1997, ApJ, 485, 92
Tresse, L., & Maddox, S. J. 1998, ApJ, 495, 691
Treyer, M., Ellis, R. S., Milliard, B., Donas, J., & Bridges, T. J. 1998, MNRAS, in press (astro-ph/9806056)
Weedman, D. 1983, ApJ, 266, 479